Journal of Applied Mechanics Vol.7,pp.1203-1212 (August 2004) JSCE

Failure mechanism of deformed concrete tunnels under plastic ground pressure

塑性地圧より変状するコンクリートトンネルの破壊メカニズム

Wei He* and Zhishen Wu**
何 偉 呉 智深

*Dr. Candidate of Eng., Dept. of Urban & Civil Eng., Ibaraki University
(4-12-1, Nakanarusawa-cho, Hitachi, Ibaraki 316-8511, Japan)
**Dr. of Eng., Professor, Dept. of Urban & Civil Eng., Ibaraki University
(4-12-1, Nakanarusawa-cho, Hitachi, Ibaraki 316-8511, Japan)

This paper presents different failure modes as well as the key variables controlling the load-carrying capacity and deformation behavior of concrete tunnels under plastic ground pressure. Based on total strain and the concept of fracture energy, a parabolic compressive softening model as well as a linear tensile softening model is introduced. It is found that the variables, such as the concrete compressive strength, concrete compressive fracture energy, soil stiffness, modes of external loads and inverts, have a great influence on structural performances of concrete tunnels. The final failure of tunnels with inverts is in the mode of compressive crushing under soil stiffness of 110 N/mm, while the final failure of that without inverts is in the mode of cracking failure. Moreover, concrete compressive strength has significant influence on the structural load-carrying capacity, while concrete compressive fracture energy affects remarkably the ductility of tunnel structures.

Key Words: *plastic ground pressure, parabolic compressive softening model, invert, compressive strength, compressive fracture energy*

1. Introduction

In many practical engineering applications involving a deformed or partially damaged concrete tunnel, except for cracking failure of concrete, concrete compressive failure is also an important structural failure mode[1]. However, due to the soil constraint and various types of external loads, deformed concrete tunnels exhibit more complicated failure modes. Therefore, different types of real external loads and their formation mechanism need to be studied to understand the behavior of deformed tunnels. In this paper, formation mechanism of fundamental kinds of plastic ground pressure is studied. The plastic ground pressure[2] caused by soil plastic initiation of so called mode 1[3], is used as externally concentrated loads in the numerical simulations.

Furthermore, the external loads, material deterioration of concrete, construction and design methods[2] are mainly responsible for the occurrence of deformed concrete tunnels. These factors often result in structural deformation, water leakage, cracking and concrete crushing of tunnels. In all cases, deformed phenomena of concrete tunnels have occurred because either a fundamental mode of failure was not recognized, or because the assessment method was carried out by extrapolation from existing precedent without a proper understanding of the variables controlling the behavior of concrete tunnel linings or surrounding media. For example, concrete pouring quality of the inverts often has obvious influence on structural deformation behavior and failure modes. On the other hand, conventional assessment methods treat the predication of tunnel wall displacements and the estimation of ground pressure on tunnel linings separately. The most severe limitation of those approaches stems from the fact that the assumed behavioral mode may not correspond to the actual mode encountered. Most of the difficulties resulted from the lack of a valid analytical framework, which permits designers to identify key variables controlling different failure modes, load-carrying capacity and deformation behavior of concrete tunnels. Therefore, different failure modes of concrete tunnels under different boundary

conditions are studied in this paper. Moreover, this paper identifies some essential factors and key variables, which influence the deformation behavior and ultimate load-carrying capacity of concrete tunnels.

The layout of this paper is as follows. Firstly, for a better understanding of external concentrated loads namely the plastic ground pressure, the formation mechanism of different types of plastic ground pressure is studied. It helps to identify the causes of deformed tunnels as well as the conditions for their occurrence. Secondly, the details of experimental setup, experimental results of the concrete tunnel are briefly described. Thirdly, the simulation model, especially for the parabolic compressive strain softening model based on total strain, is introduced. Finally, using the finite element analysis, the concrete tunnel is modeled in a two-dimensional design space assuming a plane stress condition. In the simulation parts, different failure modes of the concrete tunnels are studied. The following aspects are also discussed: 1) effect of inverts on compressive behavior of the concrete tunnel; 2) soil stiffness; 3) concrete compressive fracture energy; and 4) concrete compressive strength.

2. Formation mechanism of plastic ground pressure

In environment with swelling of cohesive soil as well as the excavation of tunnels, stress redistribution is triggered. Usually, the stress redistribution involves a decrease in radial and an increase in tangential ground stresses.

In Fig.1, σ_h is horizontal initial ground stress, σ_v is vertical initial ground stress, and far-field stress ratio K_0 is σ_h/σ_v. When the difference between tangential (σ_θ) and radial (σ_r) stresses exceeds the soil shear strength, the plastic state of soil is induced. Moreover, this results in so-called plastic ground pressure acting on tunnel linings. Three modes of soil plastic state initiation (Mode 1, 2 and 3)[3] are indicated in Fig.2. For $K_0 < 1.0$, due to excavation or unenough support pressure, with the decrease of internal pressure, the stress difference ($\sigma_r - \sigma_\theta$) becomes larger at the spring line and mode 1 with soil plastic state at the spring line is initiated. For K_0 near 1, the stress difference ($\sigma_r - \sigma_\theta$) grows everywhere at the same rate and mode 2 with soil plastic state around the entire periphery of the tunnel develops. For $K_0 > 1.0$, initiation of soil plastic state occurs at the roof and floor of the tunnel, because of high initial horizontal stresses (mode 3).

The formation of soil plastic state will result in different types of plastic ground pressure, which will act on tunnel linings as external loads. This paper primarily adopts the plastic ground pressure caused by mode 1, based on common encounter in soft ground tunneling as well as the experiments carried out by Railway Technical Institute of Japan[4].

Furthermore, after soil plastic state is initiated, further stress relief leads to a propagation of the soil plastic zones, and localized soil plastic zones may formed, which result in more complicated types of plastic ground pressure. This will be not discussed in this paper.

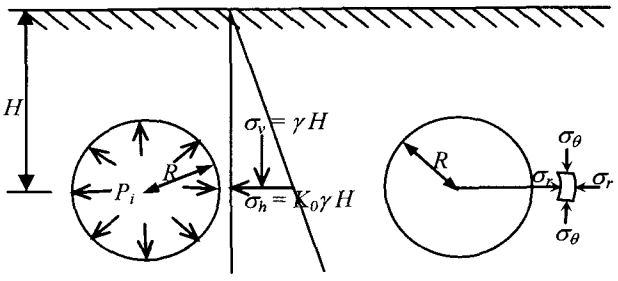

P_i: internal pressure
σ_v: vertical initial ground pressure
σ_h: horizontal initial ground pressure
K_0: far-field stress ratio
γ: unit weight of soil
σ_r: radial stress
σ_θ: tangential stress

Fig.1 Stress state of circular tunnel

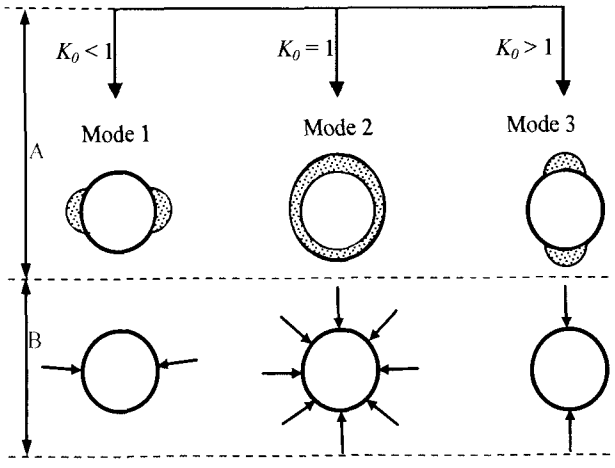

A: Initiation of soil plastic state
B: Plastic ground pressure

Fig.2 Formation mechanism of plastic ground pressure

3. Experimental Review[4]

In the following, only the specimen, setup and results, which are numerically investigated in this paper, are shown.

3.1 Experimental Specimen and Setup

A series of 1/30 model experiments was carried out by the Railway Technical Institute of Japan, in order to investigate the compressive behavior and different failure modes of concrete tunnel linings with different boundary

conditions. Considering the practical stress state, the load conditions in the experiments include not only concentrated loads, but also the soil constraint outside tunnel linings; therefore, this experimental study gave more care about the interaction between the concrete tunnel lining and soil constraint.

Considering surrounding soil constraint, a kind of constraining equipment is used in the experiment to simulate the outside soil, as illustrated in Fig.3. The rubber bearings that are set outside the concrete tunnel lining provide constraint to the outward deformation. The horizontal direction of the tunnel lining at the floor is constrained by springs or steel stopper. The external load is acted diagonally at the outside crown, which is transferred by a steel bolt from the oil pressure load machine to the tunnel lining specimen.

The material properties of experiments are as follows. Concrete Young's modulus is $E_c = 1.5\times10^4$ MPa, Poisson ratio is $\nu = 0.15$, tensile strength is $f_t = 2.0$ MPa, compressive strength is $f'_c = 21.0$ MPa, soil stiffness is $K_{soil} = 110$ N/mm, and the stiffness of floor constraining spring is $K_{foot} = 400$ N/mm.

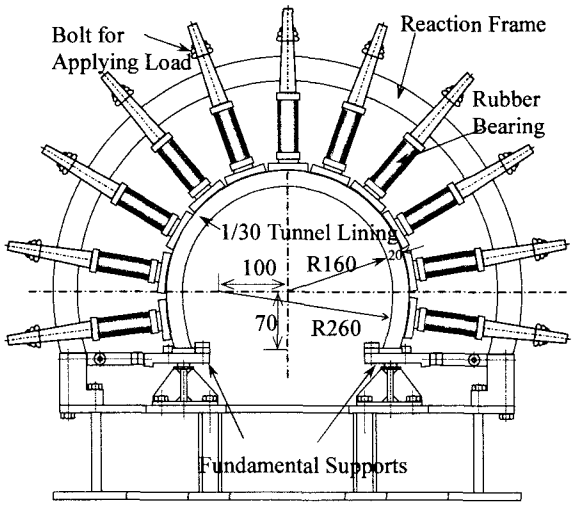

Fig.3 Concrete tunnel specimen and experimental setup (unit: mm)

3.2 Experimental Results

Two experimental cases are studied in the present paper[4]. The concentrated loads were transferred by a steel bolt from the oil pressure load machine to the tunnel lining specimen, and acted on the outside sidewalls of the concrete tunnel symmetrically, with load direction inclined to the horizontal with angle 10°. Considering the concrete pouring quality of the inverts, the drawback often exists in connection between the invert and the concrete tunnel benches. Therefore, two cases of different horizontal constraining conditions at the floor of the tunnel were considered, one is the spring horizontal constraining of which the stiffness is 400 N/mm, the other is horizontal fixed constraining, as shown in Fig.4. Load-displacement responses are shown in Fig.5. The displacement in the experimental load-displacement curves denotes the displacement at load point.

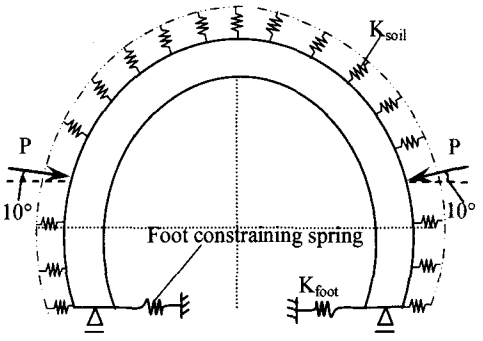

(a) Experimental case 1

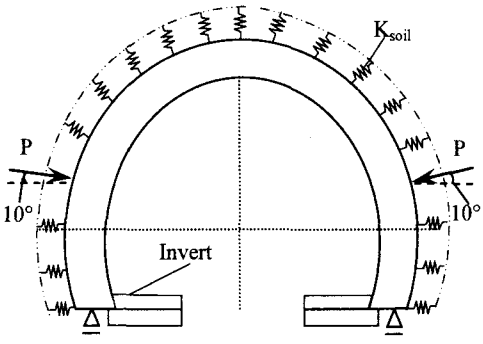

(b) Experimental case 2

Fig.4 Experimental Cases

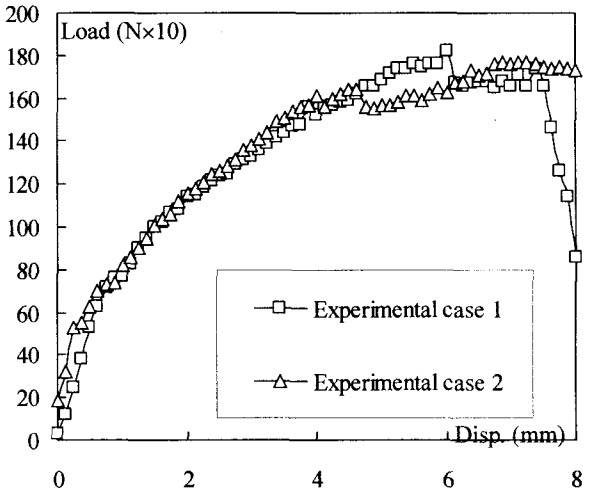

Fig.5 Load-displacement response (experimental)

4. Material Model for Concrete

The material model for concrete used in this paper is based on total strain, called the 'Total Strain Rotating Crack Model', which describes the compressive and tensile behaviors of a material with one co-rotational stress-strain relationship. It is developed along the Modified Compression Field Theory (MCFT), originally

proposed by Vecchio and Collins (1986)[5]. The three-dimensional extension to this theory is developed by Selby and Vecchio (1993)[6], and has been enhanced by Feenstra et al. (1998)[7]. The practical use of a rotating stress-strain relation requires principal stress and principal strain to be coaxial. It has been known that this coaxiality can be achieved via an implicit shear term in the rotating principal 1, 2 reference frame. Moreover, the total strain rotating crack model can be derived as a special case of the decomposed multi-directional model assuming a zero inter-crack threshold angle, so that a new crack under slightly different angle is initiated in each step while the previous cracks unload elastically. This model is very well suited for Serviceability Limit State (SLS) and Ultimate Limit State (ULS) analyses, which are predominantly governed by crushing or cracking of the material.

4.1 Compressive Behavior for Concrete

For the compressive behavior of concrete, the parabolic compressive softening model based on total strain is used in the present paper, as shown in Fig.6. In Fig.6, it shows large compressive fracture energy G_c increases the ductility of the material; while high concrete compressive strength f'_c will increase the structural strength. Thus it can be seen G_c and f'_c are important material properties, which have significant influence on the structural load-carrying capacity and deformation behavior. Therefore, here gives detailed compressive stress-strain relationship.

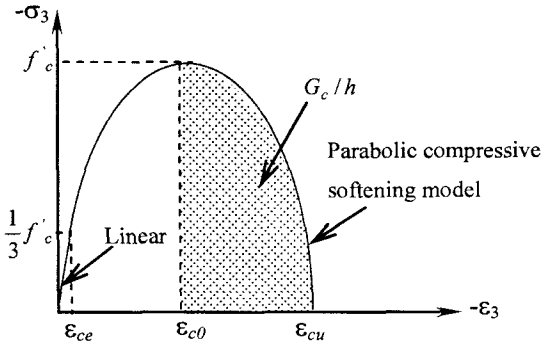

Fig.6 Concrete in compression

When concrete is loaded in compression, the response is linear until the value ($1/3\ f'_c$) of initial yield. It is as follow:

$$\sigma_3 = E_c \varepsilon_3, \qquad \text{if } 0 \le \varepsilon_3 < \varepsilon_{ce} \tag{1}$$

where E_c is concrete Young's modulus, and ε_{ce} is

$$\varepsilon_{ce} = \frac{1}{3}\left(\frac{f'_c}{E_c}\right) \tag{2}$$

where f'_c is concrete compressive strength.

In the compressive regime, the response is typically characterized by stress hardening followed by strain softening beyond the maximum attainable stress f'_c. For concrete in the direction of the largest principal compressive strain (ε_3) with compressive hardening and softening, the stress-strain relation of concrete subjected to the compression is usually expressed mathematically by a parabolic curve:

$$\sigma_3 = \begin{cases} \dfrac{f'_c}{3}\left[1+4\dfrac{\varepsilon_3}{\varepsilon_{c0}}-2\left(\dfrac{\varepsilon_3}{\varepsilon_{c0}}\right)^2\right] & \text{if } \varepsilon_{ce} \le \varepsilon_3 < \varepsilon_{c0} \\ f'_c\left[1-\left(\dfrac{\varepsilon_3-\varepsilon_{c0}}{\varepsilon_{cu}-\varepsilon_{c0}}\right)^2\right] & \text{if } \varepsilon_{c0} \le \varepsilon_3 \le \varepsilon_{cu} \end{cases} \tag{3}$$

where

$$\varepsilon_{c0} = \frac{2f'_c}{E_c} \tag{4}$$

and

$$\varepsilon_{cu} = \frac{3G_c}{2f'_c h} + \varepsilon_{c0} \tag{5}$$

with the concrete compressive fracture energy G_c and characteristic crack length h based on the element geometry. For planar elements, h is the square root of the element area.

When the stress state is in compressive-tensile condition, the major principal tensile strain, which is perpendicular to the compressive direction, may decreases the maximum attainable compressive stress f_{3max}. The reduction in the maximum attainable compressive stress f_{3max}, as a function of the coexisting transverse tensile strain ε_1, typically represents a significant softening effect. It can be evaluated by the equation:

$$f_{3\max} = \frac{f'_c}{0.8-(0.34\dfrac{\varepsilon_1}{\varepsilon_0})} \tag{6}$$

4.2 Tensile behavior for concrete

The tensile behavior of concrete can be modeled using different approaches, and one results in a more complex description than the other does. For the total strain crack model, the conventional linear softening stress-strain relation based on Mode-I fracture energy is adopted in this paper. Conditions of equilibrium and compatibility were treated in terms of average stresses and average strains. For the details, refer to Feenstra et al. (1998)[7].

4.3 Finite element constitutive model

In developing the stiffness formulations for a finite element, a material stiffness matrix $\boldsymbol{D}$ is required to relate stresses $\{\sigma\}$ to strains $\{\varepsilon\}$, that is

$$\{\sigma\} = \boldsymbol{D}\ \{\varepsilon\} \tag{7}$$

where $\{\sigma\} = [\sigma_x \sigma_y \sigma_z \tau_{xy} \tau_{yz} \tau_{xz}]$; and $\{\varepsilon\} = [\varepsilon_x \varepsilon_y \varepsilon_z \gamma_{xy} \gamma_{yz} \gamma_{xz}]$.

The form of the matrix $\boldsymbol{D}$ depends on the type of nonlinear solution algorithm employed. A secant stiffness approach is robust and stable in reinforced concrete structures with extensive cracking. However, a tangent stiffness approach has shown superiority in analysis where localized cracking and crack propagation are the most important phenomena. Based on the consideration above, the formulations that follow assume a secant-stiffness approach. This approach is according to the stiffness of an orthotropic material with zero Poisson's ratio in all directions. Moreover, the material stiffness $\boldsymbol{D}_{secant}$ is evaluated with respect to the principal axes systems. And then it must be transformed to the global axes systems. It is:

$$\boldsymbol{D} = \boldsymbol{T}^T \boldsymbol{D}_{secant} \boldsymbol{T} \tag{8}$$

where $\boldsymbol{T}$ is a transformation matrix.

For the detailed finite element formulation, refer to Feenstra et al. (1998)[7].

5. Finite Element Simulations

In finite element simulations, the concrete tunnel is modeled in a two-dimensional (2D) design space in which the structure is idealized as plane stress condition. Based on the experiments, finite element analysis is performed with **DIANA 8.1**. The concrete tunnel is discretized by plane stress elements as shown in Fig.7. The 4-node quadrilateral plane stress element is used to discretize the concrete tunnel, which is integrated at 4 Gaussian quadratic points. The line interface element is used to simulate soil constraint outside the concrete tunnel, with which the interface surface and directions are evaluated automatically from the element itself.

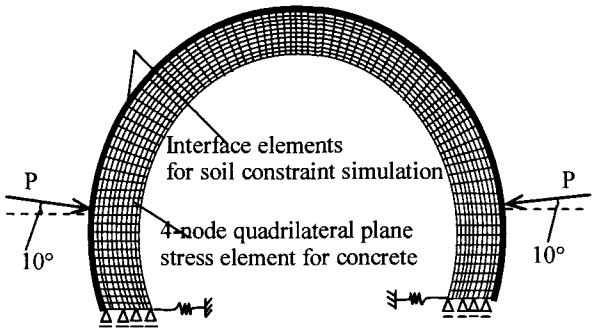

Fig.7 Structural model for finite element analysis

Table 1 Numerical Simulation Cases

Numerical Simulation Cases		Soil Stiffness K_{soil} (N/mm)	Concrete Compressive Fracture Energy G_c (N/mm)	Concrete Compressive Strength f'_c (Mpa)
With Inverts*	Without Inverts**			
Invert_Basic	Spring_Basic	110	100	14
Invert_Kc0	Spring_Kc0	0	100	14
Invert_Kc10	Spring_Kc10	10	100	14
Invert_Kc30	Spring_Kc30	30	100	14
Invert_Kc40	Spring_Kc40	40	100	14
Invert_Kc50	Spring_Kc50	50	100	14
Invert_Kc200	Spring_Kc200	200	100	14
Invert_Kc800	Spring_Kc800	800	100	14
Invert_Gc2	Spring_Gc2	110	2	14
Invert_Gc10	Spring_Gc10	110	10	14
Invert_Gc80	Spring_Gc80	110	80	14
Invert_Gc200	Spring_Gc200	110	200	14
Invert_Fc10	Spring_Fc10	110	100	10
Invert_Fc18	Spring_Fc18	110	100	18
Invert_Fc21	Spring_Fc21	110	100	21

* denotes the displacements at the tunnel floor in the x and y directions are fully constrained, and ** denotes the displacement at the tunnel floor in the x-direction is constrained via springs with stiffness of 400 N/mm, while the displacement in the y-direction is fully constrained.

In this section, based on the total strain crack model these aspects are discussed: 1) effect of inverts on compressive behavior of the concrete tunnel; 2) soil stiffness; 3) concrete compressive fracture energy; and 4) concrete compressive strength. Analyses of 1) and 2) are mainly concerned with the compressive behavior and different failure modes under different boundary conditions as well as deformation behavior of the concrete tunnel. Since the value of concrete compressive fracture energy G_c was not identified from the experiments and it is more difficult to be measured accurately than Mode-I tensile fracture energy G_f^I, it is considered as a parameter study in Analysis 3).

In the present numerical simulation analysis, the Concrete Young's modulus $E_c = 1.5\times10^4$ MPa, Poisson ratio $\nu = 0.15$, tensile strength $f_t = 2.0$ MPa and tensile fracture energy $G_f^I = 0.1$ N/mm are kept constant in all the simulation cases. The stiffness $K_{foot} = 400$ N/mm of floor constraining spring is kept constant for simulation cases without inverts. Concrete compressive fracture energy $G_c = 100$ N/mm is kept constant except that in Analysis 3). Concrete compressive strength $f'_c = 14.0$ Mpa which is identified from FEM calculation is kept constant in all simulation analyses except that in Analysis 4). Soil stiffness $K_{soil} = 110$ N/mm is kept constant except that in Analysis 2). The detailed material properties and boundary conditions are shown in Table 1. Without special explanation, the displacement in all the load-displacement curves of numerical simulations denotes the displacement of load point.

5.1 Effect of inverts on compressive behavior of the concrete tunnel

Due to the pouring quality of concrete, the drawback often exists in connection between the invert and the concrete tunnel benches, and the strength of an invert itself may lower than that of the design. So in experimental cases, two types of horizontal boundary conditions at floor of the tunnel are studied. One case is the displacement at the tunnel floor in the x-direction is constrained via springs with stiffness of 400 N/mm, while the displacement in the y-direction is fully constrained. This case is to simulate the drawback between the invert and the tunnel benches, because small relative displacement between the invert and tunnel benches often occurred if such a drawback exists. The other case is the displacements at the tunnel floor in the x and y directions are fully constrained, and this case is to simulate the perfect connection between the invert and tunnel benches.

Fig.8 shows different failure modes. Under conditions with inverts, after cracking initiation in direction of loading point (inside) followed by another two cracks which are at the sidewalls of the tunnel (outside), stabilized compressive zones are formed, and then the structure failed due to the concrete crushing (see Fig.8 d). However, under conditions without inverts, after cracking initiation in direction of loading point (inside), two cracks occurred immediately near the crown (outside); and then another two cracks, the sequence of which is named '3', initiated at the sidewalls of the tunnel (see Fig.8 b). Although compressive zones have developed as shown in (b) of Fig.8, the structure lost its load-carrying capacity quickly, due to the occurrence of the last two cracks named '5'.

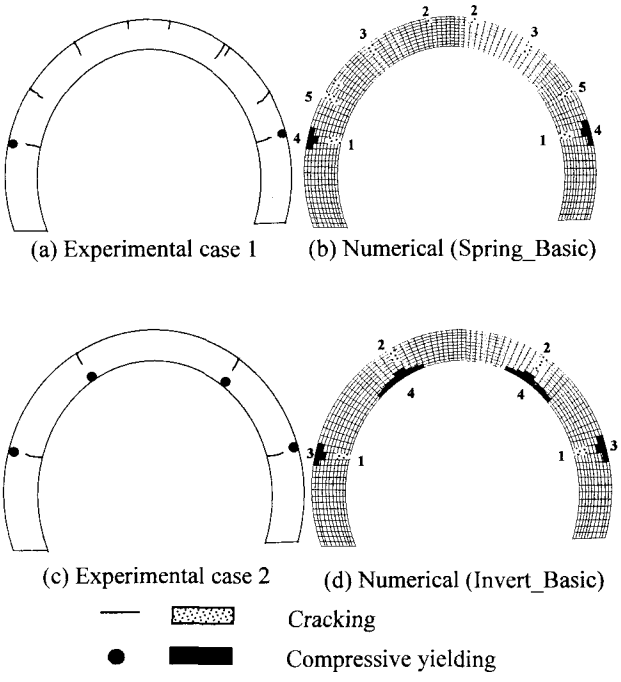

Fig.8 Compressive and cracking patterns

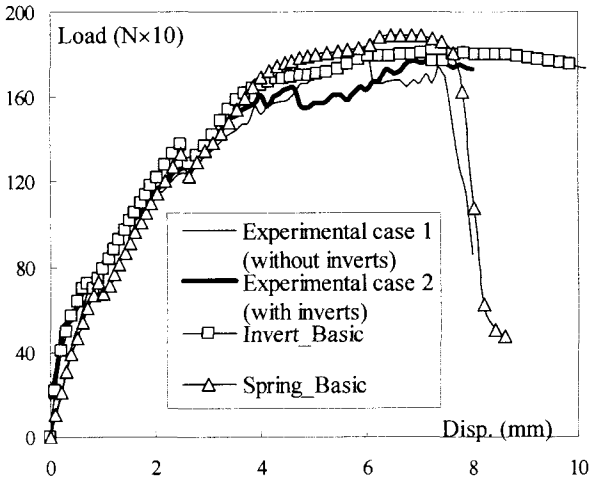

Fig.9 Effect of the inverts on structural response

In Fig.9 it shows that the initial elastic stiffness of the tunnel with inverts is higher than that of the tunnel without inverts, but the load which corresponds to the initial cracking in the tunnel is lower than that of the tunnel without inverts. The post-peak behavior of the tunnel without inverts is more brittle, because the cracks propagate one by one, which result in the structural instability and suppress the formation of stabilized compressive zones.

5.2 Soil stiffness

For the real concrete tunnel linings, the load conditions include not only concentrated external loads, but also the constraint from soil. The soil mass constrains the outward deformation of the tunnel linings. Because of the difference of soil mass density outside the tunnel linings, the constraining effects may be also different. In the simulation, this difference is reflected in the stiffness of interface elements. Several cases with different soil stiffness are presented in this section.

In Fig.10, every fully open crack corresponds with a peak on the load-displacement curve. It is found concrete crack occurs firstly at the early stage of loading (Fig.10). After a crack pattern has developed, stresses are still transferred through compressive zones in uncracked concrete, which increases the total stiffness of the structure. Meanwhile, due to the soil constraint, concrete subjected to compressive stresses shows a pressure-dependent behavior. With increasing soil stiffness, the structural strength and stiffness increase; but after soil stiffness is higher than 50 N/mm, the structural strength does not obviously increase.

In Fig.11, peak displacement means that a displacement corresponds to the structural peak load. From the numerical results in Fig.11, it is found that the difference of the peak displacement between the tunnel with inverts and that without inverts is obvious, when the soil stiffness is below 50 N/mm.

From Fig.10 and Fig.11, it shows that the structural ductility is reduced when the soil stiffness is larger than 50 N/mm. It is due to different length along the tunnel opening, which is able to accept ground pressure, as shown in Fig.12.

From the numerical results in Fig.13, it is found that the soil outside the tunnel prevents the structural cracking development with large soil stiffness. Moreover, under soil stiffness of 800 N/mm, the tunnel without inverts lost its load-carrying capacity due to the compressive failure. However, under soil stiffness of 110 N/mm, the final failure of the tunnel without inverts is cracking failure.

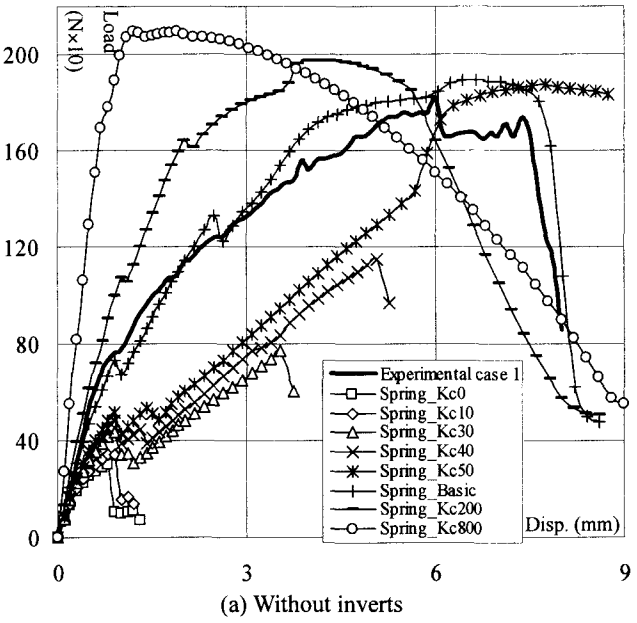

(a) Without inverts

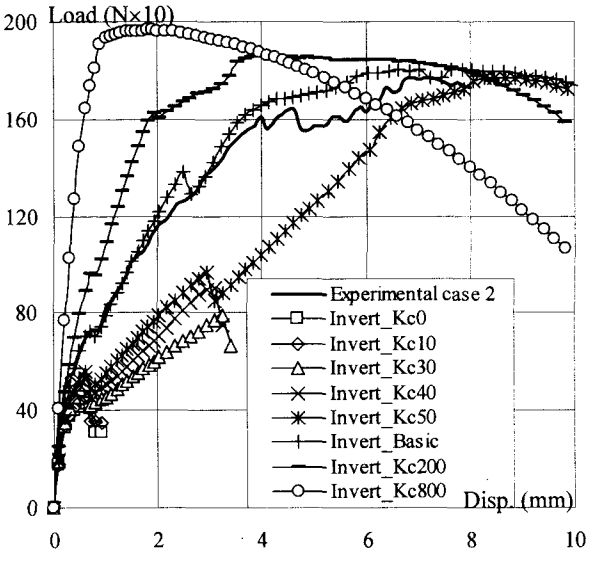

(b) With inverts

Fig.10 Effect of soil stiffness on the tunnel behavior

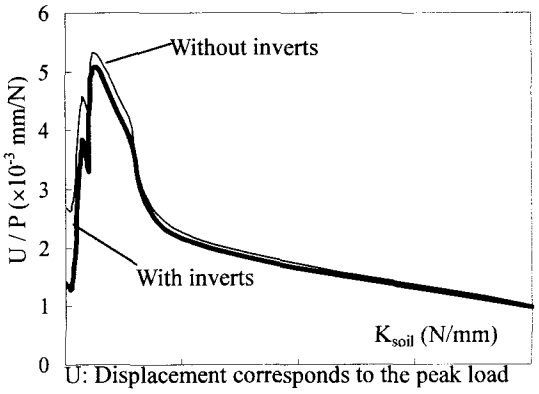

U: Displacement corresponds to the peak load

P: Peak load

Fig.11 Pressure-dependent behavior of the tunnel with different soil stiffness

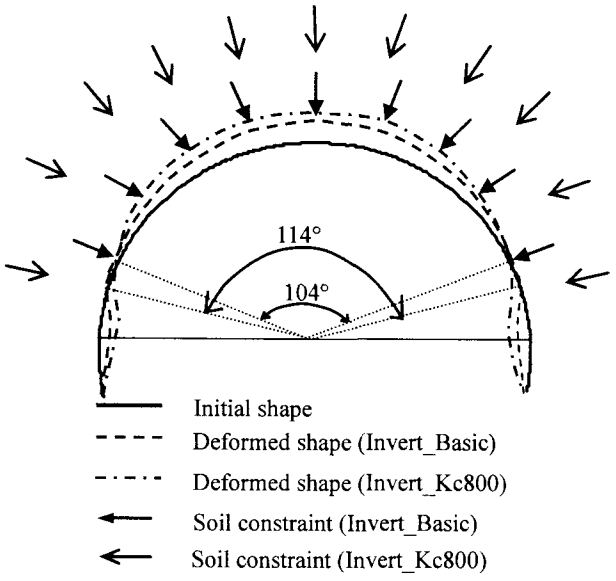

Fig.12 Deformed shape with soil constraint

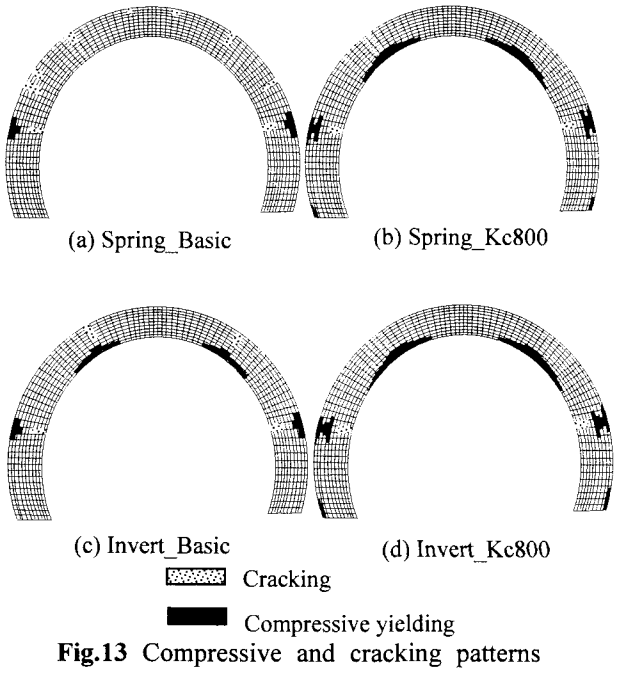

Fig.13 Compressive and cracking patterns with different soil stiffness

5.3 Concrete compressive fracture energy

Similar to concrete tensile fracture energy, the concept of released energy and equivalent length is also applied to model compressive behavior by introducing a compressive fracture energy G_c, although it is recognized that compressive failure is physically more a volume-driven process than a surface-driven process. The compressive fracture energy is considered as a material property, but it's due to lack of information of this property, and the compressive failure is more complex than tensile failure, so cases with compressive fracture energy G_c = 2, 10, 80, 100 and 200 N/mm are studied, with constant compressive tensile strength f'_c = 14 MPa.

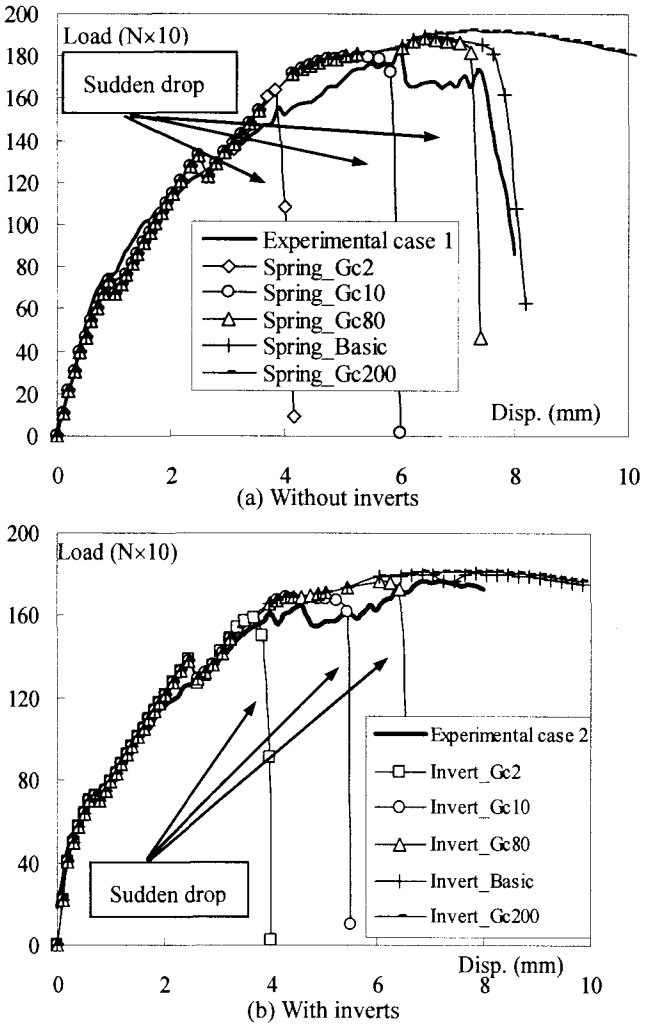

Fig.14 Compressive strain softening behavior with different compressive fracture energy

In Fig.14, it shows sudden-drop phenomenon in post-peak regime, when the small compressive fracture energy is taken. This comes from two aspects. One reason is that small compressive fracture energy will cause too little compressive softening stiffness. The local crushing failure only occurs in several elements to introduce temporarily unstable behavior in the overall response of the model, as shown in Fig.15 (a). Therefore, the presence of this type of response in the analysis model usually indicates the compressive fracture energy is unreasonably low. Another possible reason is that, from the viewpoint of numerical calculation and for the rotating stress-strain relation, the determination of the principal directions should also include a procedure to determine and avoid sudden re-ordering of the principal axes. The ordering of the principal strain axes is assumed spurious when the updated directions are not closest to

the previous principal directions. If sudden rotation of principal directions occurs, the ordering of the principal axes is may erroneous, and the convergence of the calculation will deteriorate dramatically.

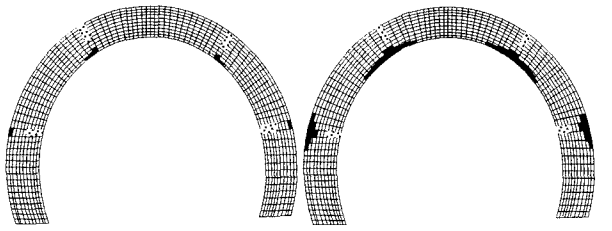

(a) The case of Invert_Gc2 (b) The case of Invert_Gc200

Compressive yielding

Cracking

Fig.15 Compressive and cracking patterns with different compressive fracture energy

Although the compressive fracture energy only controls the stiffness of compressive strain descending branch, the ultimate load-carrying capacity of structures may be influenced by compressive fracture energy, due to the reasons above. The numerical results in this section show that G_c = 100 N/mm is preferred by comparison between numerical results and experimental ones, as shown in Fig.14. At the same time, the large value of compressive fracture energy makes the structure more flexible in post-peak regime.

5.4 Concrete compressive strength

Due to the randomness and different conditions during pouring the concrete specimens, such as temperature, humidity, drying time, component ratio and the scale of structures, the strength of concrete, especially the compressive strength may vary, and it may has significant influence on the structural response of tunnel.

In this section, the cases with different compressive strength f'_c = 10, 14, 18 and 21 MPa are studied, but the concrete compressive fracture energy is kept constant as G_c = 100 N/mm. From the numerical results (see Fig.16), it shows concrete compressive strength has significant influence on the ultimate load-carrying capacity of the tunnel, different from the effect of compressive fracture energy (see Fig.17). The high concrete compressive strength increases the structural strength. Therefore, the guarantee on compressive strength is considered to be important in plain concrete tunnel linings. Meanwhile, for the compressive fracture energy is kept constant, the high concrete compressive strength decreases the ductility of the structure.

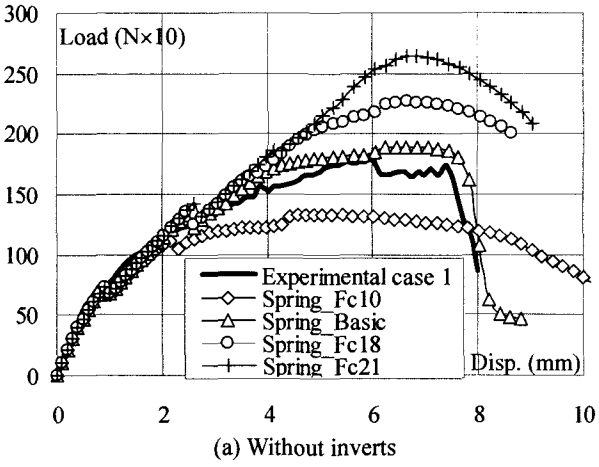

(a) Without inverts

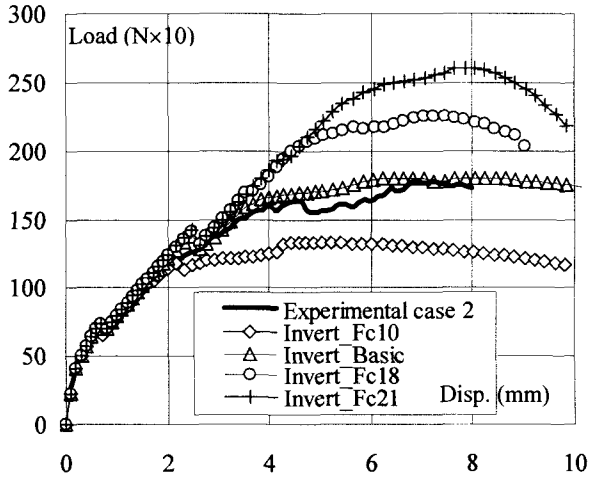

(b) With inverts

Fig.16 Load-displacement response with different compressive strength

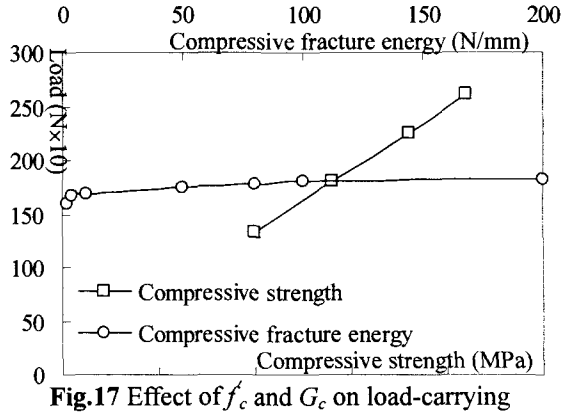

Fig.17 Effect of f'_c and G_c on load-carrying capacity (with inverts)

6. Conclusions

Under plastic ground pressure as well as soil constraint, different failure modes of deformed concrete tunnels are studied. Some numerical simulations have been carried out to investigate the compressive and cracking behavior of 1/30 scale model of the concrete tunnel. From the case studies, the following conclusions are drawn:

(1) The final failure of deformed concrete tunnels depends on the compressive behavior of concrete as well as the crack patterns. Furthermore, except for material properties of concrete, the structural dominant failure modes seriously depend on soil stiffness and inverts, when tunnels are subjected to plastic ground pressure. The final failure of the tunnel without inverts is compressive failure, when soil stiffness is 800 N/mm, but when soil stiffness is 110 N/mm, the final failure of that is cracking failure.

(2) The key variables are concrete compressive strength, concrete compressive fracture energy, soil stiffness, modes of external loads and inverts. These factors control not only the structural deformation behavior but also the load-carrying capacity.

(3) A comparison of the numerical results with the experimental ones indicates a good agreement of the load-displacement relationship and also a good prediction of the different failure modes. It shows the parabolic compressive softening model based on total strain and concept of fracture energy is rational and effective to assess the compressive behavior and load-carrying capacity of deformed tunnel linings.

(4) Under plastic ground pressure based on soil plastic initiation of mode 1, inverts of tunnels have obvious influence on the structural failure modes as well as the structural deformation behavior. The final and dominant failure of the concrete tunnel with inverts is a compressive failure when soil stiffness is above 110 N/mm; while without inverts, the tunnel fails due to propagation of multiple cracks, which results in the geometrical instability of the structure, when soil stiffness is less than 110 N/mm. Inverts are helpful to increase the structural initial stiffness, while the lack of inverts does not.

(5) In plain concrete tunnel linings, the concrete compressive strength has main influence on the structural load-carrying capacity. High concrete compressive strength will increase the structural ultimate load-carrying capacity.

(6) The concrete compressive fracture energy has obvious effect on the structural deformation behavior in post-peak region. Large concrete compressive energy increases the structural ductility; but it has no significant effect on the structural ultimate load-carrying capacity. Furthermore, due to lack of information of compressive fracture energy, the preferred value is 100 N/mm in parameter studies as well as comparison between the numerical simulation results and the experimental ones.

(7) The soil constraint outside concrete tunnels plays an important role in controlling the compressive and deformation behavior as well as crack propagation of concrete. When soil stiffness is below 50 N/mm, the structural stiffness, ductility and strength are increased obviously; while with the value above 50 N/mm, the structural strength is not increased significantly. Moreover, high soil stiffness is helpful to prevent the crack localization and its development.

(8) For the structural failure due to the deficient strength of inverts, strengthening of the inverts is helpful to increase the structural strength of the deformed tunnels.

(9) The cracks often induce further deterioration of deformed tunnels, therefore, the inner reinforcement by steel plate or carbon fiber sheet is suggested in the maintenance.

References

1) He, W., Wu, Z. S., Yin, J. and Kojima, Y., Compressive failure of concrete tunnel lining simulated by different compressive models, *Journal of Applied Mechanics, JSCE,* Vol.6, pp.1207-1215, 2003.

2) JSCE, *Tunnel Deformation Mechanics*, Japan Society of Civil Engineers, 2003. (in Japanese)

3) Wong, R. C. K. and Kaiser, P. K., Performance Assessment of Tunnels in Cohesionless Soils, *Journal of Geotechnical Engineering, ASCE,* Vol.117, No.12, pp.1880-1901, 1991.

4) Asakura, T., Kojima, Y. and Ando, T., Analysis of the behavior of tunnel lining – Simulation of experimental results on double track tunnel lining, *Tunnel Engineering Research Presentation Meeting, Paper and Report Collection,* Vol.1, pp. 183-188, 1991.

5) Vecchio, F. J. and Collins, M. P., The modified compression field theory for reinforced concrete elements subjected to shear, *ACI Journal, Proceedings*, Vol.83, No.2, pp.219-231, 1986

6) Selby, R. G. and Vecchio, F. J., Three-dimensional Constitutive Relations for Reinforced Concrete, *Tech. Rep. 93-02, Univ. Toronto, dept. Civil Eng., Toronto, Canada*, 1993.

7) Feenstra, P. H., Rots, J. G., Arnesen, A., Teigen, J. G., and Hoiseth, K. V., A 3D constitutive model for concrete based on a co-rotational concept, *Computational modeling of concrete structures, Proc. EURO-C,* pp.13-22, 1998.

(Received: April 16, 2004)